JOURNAL OF GEOPHYSICAL RESEARCH, VOL. 112, A11212, doi:10.1029/2006JA012191, 2007

Jovian *S* burst generation by Alfvén waves

S. Hess,[1,2] F. Mottez,[1] and P. Zarka[2]

Received 24 November 2006; revised 28 March 2007; accepted 25 July 2007; published 16 November 2007.

[1] Jupiter's radio emissions are dominated in intensity by decametric radio emissions due to the Io-Jupiter interaction. Previous analyses suggest that these emissions are cyclotron-maser emissions in the flux tubes connecting Io or Io's wake to Jupiter. Electrons responsible for the emission are thought to be accelerated from Io to Jupiter. We present simulations of this hot electron population under the assumption of acceleration by Alfvén waves in the Io flux tube. Outside of limited acceleration regions where a parallel electric field associated with Alfvén waves exists, the electrons are supposed to have an adiabatic motion along the magnetic field lines. Near Jupiter a loss cone appears in the magnetically mirrored electron population, which is able to amplify extraordinary (X) mode radio waves. The X-mode growth rate is computed, which allows us to build theoretical dynamic spectra of the resulting Jovian radio emissions, whose characteristics match those observed for Jovian *S* bursts.

Citation: Hess, S., F. Mottez, and P. Zarka (2007), Jovian *S* burst generation by Alfvén waves, *J. Geophys. Res.*, *112*, A11212, doi:10.1029/2006JA012191.

1. Introduction

[2] The motion of the satellite Io across Jovian magnetic field lines in the plasma torus surrounding its orbit provides an important and continuous energy source for electron acceleration, ultimately generating intense decametric radio emissions [*Queinnec and Zarka*, 1998] and bright UV spots at the Io flux tube (IFT) footprint [*Prangé et al.*, 1996]. The electric field generated by this motion is thought to induce electric currents and/or Alfvén waves [*Goldreich and Lynden-Bell*, 1969; *Neubauer*, 1980; *Saur*, 2004] which may both accelerate electrons in the plasma torus and in the Io flux tube (IFT). Owing to the magnetic mirror effect near the Jovian ionosphere, these electrons acquire an unstable distribution relative to the cyclotron-maser instability (CMI) [*Wu and Lee*, 1979; *Louarn*, 1992].

[3] Millisecond (or *S*) bursts are discrete and intense emissions occurring near the electron cyclotron frequency and drifting in the frequency-time plane. Figure 1 shows a typical dynamic spectrum of these emissions. Their source propagate like electrons in quasi-adiabatic motion moving along the magnetic field lines away from Jupiter [*Ellis*, 1965; *Zarka et al.*, 1996; *Hess et al.*, 2007]. Burst occurrence seems often quasi-periodic with a rate of few tens of Hz. The discrete nature of the *S* bursts and their quasi-periodicity, originating from a continuous excitation, is investigated in the present paper. *Ergun et al.* [2006] proposed that Alfvén waves (AW) could resonate near the Jovian ionosphere, accelerate electrons periodically and thus produce periodic bursts.

[4] Using these waves as the source of free energy, we simulate electron acceleration by Alfvén waves along the Io flux tube (IFT) and we deduce the CMI growth rates from their distribution. Then we compare the time/frequency evolution of the maximal value of the growth rate with the dynamic spectra previously recorded from the ground.

[5] We assume that the CMI is responsible for the emissions since it is observed in many auroral contexts, in particular the earth auroral kilometric radiations. Other processes have been proposed to explain Jovian burst emissions. *Ryabov* [1994] proposed a mechanism in which the emissions are due to the curvature radiation. This model explains many *S* bursts properties but requires electrons with an energy above 10 MeV which have not been seen on in situ measurements. *Zaitsev et al.* [1985] proposed a model of nonlinear conversion between plasma waves and extraordinary mode waves. *Willes* [2002] proposed a phase bunching feedback model which explains some atypical features of the *S* bursts, in particular their interaction with others Jovian emissions (*L* bursts), but it is still at a qualitative stage. *Calvert et al.* [1988] proposed a model of natural lasing in which the laser cavity expand with Io's motion around Jupiter. The two latter models suppose that the source moves at a velocity different from the velocity of the electrons, but *Zarka et al.* [1996] and *Hess et al.* [2007] showed that in most cases *S* bursts drift according to an adiabatic motion of the emitting electrons. *Wong and Goldstein* [1990] showed that bursty emissions can be generated by a strong temperature anisotropy, but the radio beaming ($\leq 30°$) is very different from the one deduced from observations [*Queinnec and Zarka*, 1998] ($\geq 70°$). The microsecond pulse structure of the *S* bursts discussed by *Carr and Reyes* [1999] may describe phenomenon with a timescale far shorter than those in which we are

[1] Laboratoire de l'Univers et de ses Thories, Observatoire de Paris, Centre Nationale de Recherche Scientifique, Meudon, France.

[2] Also at Laboratoire d'Etudes Spatiales d'Instrumentation en Aerophysique, Observatoire de Paris, Centre Nationale de Recherche Scientifique, Meudon, France.

0148-0227/07/2006JA012191$09.00

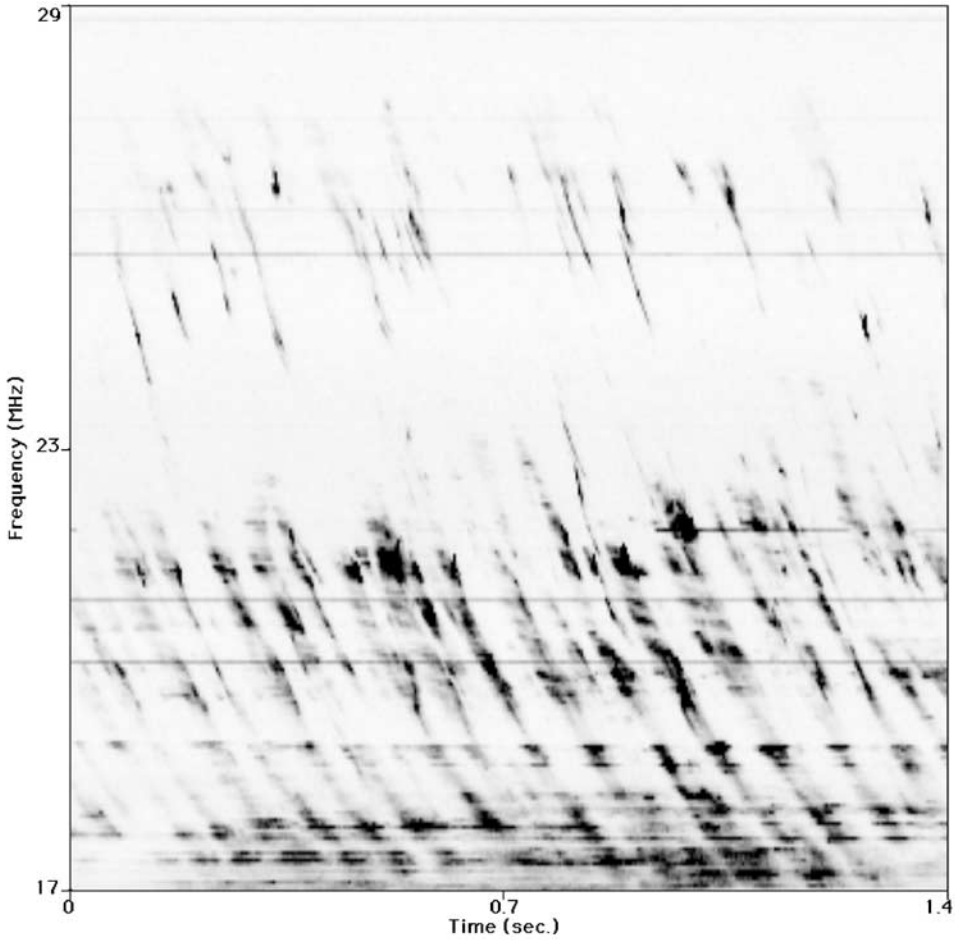

Figure 1. Dynamic spectrum recorded at the Nançay decameter array in April 1995. The drifting structures are Jovian *S* bursts. They show a negative drift rate of about −20 MHz/s, corresponding to the antiplanetward adiabatic motion of the emitting electrons. Even if the bursts do not repeat periodically, the mean time between each bursts remains about 70 ms.

interested and are not a constraint for ''millisecond'' burst generation mechanism. This short discussion (more developed in *Zarka* [1998]) justifies our choice of the CMI mechanism.

[6] We use a particle test code to compute particles motion along the IFT (section 2.1). External fields, computed on a grid, are described in section 2.2. The introduction of Alfvén waves is discussed in section 3 and CMI growth rate computations in section 4. Results are presented in section 5 and discussed in section 6.

2. Description of the Simulation

2.1. Particle Motion and Injection

[7] We simulate the motion of electron guiding–centers in imposed (not self-consistent) electromagnetic and gravitational fields. The equation of motion is given by the conservation of the magnetic moment μ and by the gradients of the electric potential ϕ_E and the gravitational (and inertial) potential ϕ_G.

$$\mu = v_\perp^2/B = const. \tag{1}$$

$$\frac{dv_\parallel}{dt} = -\nabla\left(\frac{q}{m}\phi_E + \frac{\mu}{m}B + \phi_G\right) \tag{2}$$

[8] In our simulation we simulate only the hot component of Io's electron population (i.e., population with a thermal velocity about 200 eV measured by Voyager and Galileo [*Bagenal*, 1994; *Moncuquet et al.*, 2002]). A constant number of particles (∼700 at each time step) is injected at the Io boundary to get a constant injection flux. The particles can exit the simulation at both ends of the grid. Our simulation is made with 6.4×10^7 particles on a 4096 cells grid. The length of a grid cell is $\Delta x = 114$ km $\simeq 1.16 \times 10^{-3}$ R_J; therefore the total length of the system is $L = N\Delta x = 6.5$ R_J.

2.2. External Fields

[9] The permanent magnetic field is computed using the VIP4 multipolar magnetic model of Jupiter [*Connerney et al.*, 1998]. This model was built from in situ magnetic field measurements of Voyager and Pioneer, and from infrared observations of the position of the IFT footprints on Jupiter. Up to now, this is the most accurate published model for the computation of the magnetic field in the IFT.

Table 1. Density at the Simulation Grid Boundaries[a]

Species	Density, cm^{-3}	Temperature, eV
At Io's Boundary		
Emitting electrons	1	200
Cold electrons	1250	5
Oxygen II	1000	$T_\perp = 2T_\parallel = 70$
Sulfur II	250	50
Io's protons	1	200
At Jovian Boundary		
Ionospheric electrons	2.10^5	0.31
Ionospheric protons	2.10^5	0.31
Secondary electrons	150	100

[a]From *Su et al.* [2003, Table 2.2].

[10] Io-controlled Jovian radio emissions occur only when Io's longitude lies in a specific range of nearly 160° to 300° (so called "active" longitude) [*Carr et al.*, 1983; *Queinnec and Zarka*, 1998]. We choose here to simulate the magnetic field line in the northern hemisphere whose longitude at equator is 230°. This value corresponds to the so-called "Io-B" emissions which are the strongest sources of Io-controlled emissions.

[11] The gravitational (and inertial) potential ϕ_G is given by the Jovian attraction and the centrifugal potential. Io's attraction is neglected. Thus:

$$\phi_G = \frac{GM_J}{R} + \frac{\Omega^2 R^2}{2} \tag{3}$$

where M_J is Jupiter's mass and Ω is Jupiter's angular rotation rate.

[12] We estimate the ambipolar electric potential ϕ_E resulting from the gradient of the gravitational potential ϕ_G only. We compute the densities of all the species present in the IFT (see Table 1). First of all we calculate the distribution f_α of each species α along the IFT from its distribution at its injection boundary x_b. From Liouville's theorem we get:

$$f_\alpha\left(v_b^2, \mu, x_b\right) = f_\alpha\left(v_1^2, \mu, x\right) = f_\alpha\left(v_b^2 + \delta v^2, \mu, x\right) \tag{4}$$

where δv^2 is the variation of kinetic energy between the positions x_b and x. It can be expressed in terms of potentials variations between x_b and x.

$$\delta v_\alpha^2 = \frac{2q_\alpha}{m_\alpha}\left(\phi_{E,x} - \phi_{E,x_b}\right) + \phi_{G,x} - \phi_{G,x_b} \tag{5}$$

is negative since the electrostatic force is weaker than the gravitational force from which it is derived. Then the total density is (using equation (4)):

$$\rho_\alpha(\phi_E, \phi_G, x) = \int_0^\infty f_\alpha(v2, \mu, x) dv2 \tag{6}$$

$$\rho_\alpha(\phi_E, \phi_G, x) = \int_{-\delta v2}^\infty f_\alpha(v_b2 + \delta v2, \mu, x) dv_b2 \tag{7}$$

$$\rho_\alpha(\phi_E, \phi_G, x) = \int_{-\delta v2}^\infty f_\alpha(v_b2, \mu, x_b) dv_b2 \tag{8}$$

[13] For Maxwellian distributions we get:

$$\rho(\phi_E, \phi_G, x) = \sum_\alpha \rho_\alpha(x_b) exp\left(\frac{\delta v2_\alpha}{v_{T,\alpha}^2}\right) \tag{9}$$

where $v_{T,\alpha}$ is the thermal velocity of the specie α. The density includes the contribution of Jovian ionospheric particles below the altitude corresponding to the minimum of the gravitational potential ϕ_G (range dominated by the ionospheric species) and of Io torus particles above that altitude (range dominated by the torus species). The densities at boundaries (Table 1) are taken from *Su et al.* [2003].

[14] Quasi-neutrality imposes $\rho(\phi_E, \phi_G, x) = 0$, thus we minimize the total charge density by iteration with a gradient method to obtain an estimation of the electric potential $\phi_{E,n}$ at each point $x = n\Delta x$ of the simulation grid:

$$\phi_{E,n+1} = \phi_{E,n} + \frac{\rho\left(\phi_{E,n}, \phi_G, x\right)}{\left(\frac{\partial \rho\left(\phi_{E,n}, \phi_G, x\right)}{\partial \phi_{E,n}}\right)} \quad (\textit{Iteration over } n) \tag{10}$$

Moreover it allows for the plasma density (and temperature) profiles which are also used below to compute the Alfvén waves velocity.

[15] A more sophisticated computation of the electric potential and species density has been made by *Su et al.* [2003] under the assumption of a large electric potential difference imposed between Io and Jupiter. They obtain a localized potential drop about 30 kV near one Jovian radius above Jupiter, leading to electron energy agreeing with precipitating electrons (auroral spot generators), but much larger than observed for the radio emissions (~5 keV in the work of *Zarka et al.* [1996] and *Hess et al.* [2007] from the *S* bursts drift rate) and too large for our simulation. However, even if the electric potential profile is different, the density profile and the related Alfvén speed we found are qualitatively the same as those found in the work of *Su et al.* [2003]. Concerning the electron acceleration, the processes are different. In our paper, the free energy for acceleration does not come from an imposed potential drop at the boundaries but from Alfvén waves that we force into the system.

3. Alfvén Waves

[16] In ideal MHD, Alfvén waves have a wavelength $\lambda \ll \rho_s$ and $\lambda \ll \lambda_e$ where ρ_s is the ion acoustic gyroradius and λ_e is the electron skin depth, and they carry only a perpendicular electric field. Thus they cannot accelerate electrons. In the case of shorter wavelength, the kinetic Alfvén wave theory [*Lysak and Song*, 2003] shows that the Alfvén waves can carry a parallel electric field. As our simulation scheme does not allow for self-consistent electromagnetic fields, the Alfvén waves and their associated parallel electric fields are computed analytically. The waves group velocity (relativistic Alfvén velocity v_a) is:

$$v_a = \left(c^2 + \frac{\mu_0 \rho}{B^2}\right)^{-1/2} \tag{11}$$

and the phase velocity v_ϕ:

$$v_\phi = v_a \sqrt{\frac{1 + k_\perp^2 \rho_s^2}{1 + k_\perp^2 \lambda_e^2}}. \tag{12}$$

[17] The perpendicular wavelength $\lambda_\perp$ is proportional to the flux tube section (i.e., to $B^{1/2}$) with a value of ~10 km at the Jovian surface in our simulation. The parallel electric field generated by a kinetic Alfvén wave has been computed by *Lysak and Song* [2003]. In the cold electron case it can be simplified in:

$$\delta E_\parallel \simeq \omega_a k_\perp \lambda_e^2 \delta B_\perp \tag{13}$$

where ω_a is the Alfvén wave frequency.

[18] Figure 2 shows the parallel electric field generated by Alfvén waves during the simulation. We introduce near Io's torus border (1.6 R_J from Io) a planetward Alfvén waves train during 3 s. The parallel electric field amplitude increases until an altitude of ~2 R_J and decreases abruptly near the Jovian ionosphere. It becomes negligible enough so that the particles can be considered following an adiabatic motion below 2 R_J. Waves are reflected near the Jovian ionosphere. *Su et al.* [2006] showed that Aflvèn waves resonate near Jupiter at a frequency about 20 Hz and can thus generate quasi-periodic bursts. Owing to too large space and time steps, the present simulation does not allow us to observe such a phenomenon. For this reason, we introduce an Aflvén waves train with a frequency of only 5 Hz. The introduced wave has an amplitude of about 10^{-2} Gauss which is enough to generate an electric field strong enough to accelerate the electron to an energy of a few keV.

[19] Figure 3a shows what kind of distribution function is expected in order to trigger the cyclotron maser instability, that we be considered in the next section. This kind of distribution function is characterized by two important features: a loss cone with a positive gradient, or a beam, along the border of the loss cone, and a shell distribution.

[20] Figures 3b and 3c show the electron distribution function derived from our simulation, with an Alfvén wave, recorded at an altitude $z = 0.1\ R_J$, at times $t \simeq 5$ sec. and $t =$ 8 sec.. We can seen on them the features required for cyclotron-maser instability. Other plots of the distribution function (not displayed here) show that the distribution function is modulated, almost periodically, at the frequency (5 Hz) of the input Alfvén wave.

[21] We can see in Figures 3b and 3c, the loss cone in the upward (Io-ward) particle distribution, it is a consequence of low pitch angle particles capture in the Jupiter ionosphere. There is also a partial shell that mainly concerns downgoing particles. This shell results from downward particle acceleration combined with pitch angle diffusion caused by magnetic mirroring. In Figure 3c, we can see also a beam of accelerated particles near the loss cone border. Comparison with other figures shows that this beam, as well as the partial shell, are modulated with a ~5 Hz frequency. The beam near the loss cone and the shell both correspond to velocities of the order of 0.1 c; that is, kinetic energies $E \sim$ 3 keV. How can such particles, with an initial energy of about 200 eV ($v \sim 0.03$ c), have been accelerated up to 3 keV ($v \sim 0.11$ c)?

[22] Many theories of the formation of beam by kinetic AW involve wave-particle resonance and require that the particles of the beam have a velocity close to the Alfvén wave velocity in the acceleration region [*Kletzing*, 1994; *Su et al.*, 2004]. In our simulation, at low altitude were acceleration is expected, ($V_A \sim 0.8$ c), the Alfvén wave phase velocity given by equation (12) is $v_\phi \sim 0.2-0.4$ c, well above the velocities of the unaccelerated and accelerated electrons. Thus acceleration is not a result of resonant wave-particle interaction. Can we explain the efficiency of the electron acceleration by AW in spite of not being resonant? Electron beam formation with non resonant particles has already been studied in the context of Earth auroral acceleration, using self-consistent PIC simulations [*Génot et al.*, 2000, 2004]. It appears that in spite of their high phase velocity, the AW have quite a long-wavelength λ, and therefore a long period. We have already mentioned that we have set a frequency of 5 Hz; that is, a period of 0.2 s. When electrons can see a parallel electric field oscillating at a such low frequency, they can be accelerated, in both directions, for time lapses of about 0.05 s, that is quite long for electrons. On this timescale (that correspond to a quarter of AW period), an upward electric field cause a global heating and a bulk acceleration of the electrons. Half an AW period later, an opposite electric field cause a bulk acceleration in the opposite direction, and increases electron heating. As the acceleration/heating region has a finite extent, the fastest particles escape this region and form a beam. In the Earth auroral context studied by *Génot et al.* [2000, 2004], the accelerated particles can go faster than the AW, and the beam is formed by supra-Alfvénic particles running away from the $\lambda/4$ long region where they were accelerated. In the present context, the accelerated particles (at $v \sim 0.11$ c) are infra-Alfvénic and such a runaway cannot explain beam formation. However, in our simulations, acceleration occurs at low altitude, in the neighborhood of the wave reflection region. The acceleration region is therefore limited at low altitude, because the AW stops to generate a parallel electric field. We can therefore interpret the downward beam as a consequence of heated electrons, running downward when $E_\parallel$ is upward, and escaping the AW region before $E_\parallel$ reverses direction. We can roughly estimate the length of the acceleration region: during a half of an AW period, $\delta t \sim 0.1$ s, downgoing particles at $v \sim$ 0.11 c have time to quit the acceleration region. The length

Figure 2. (a) Parallel electric field associated with Alfvén waves. The Alfvén wave train is injected near the torus border (altitude ~5 R_J). Its maximum value is reached for an altitude of ~2 R_J, above the emissions region (<0.5 R_J) but far away from the Io torus. (b and c) The dynamic spectrum of the loss cone instability growth rate. From time 0 s (Alfvén wave introduction) to 4 s (Figure 2b) and from 4 to 8 s (Figure 2c). The background (owing to permanent loss cone) is subtracted. In order to show clearly the radio structures, only growth rates above the background are shown in Figure 2c. Low-frequency structures appearing slightly before 2 s (in Figure 2b) correspond to the Alfvén waves passage and are due to bulk acceleration. They appear mainly in absorption (negative growth in Figure 2b). After 5 s, drifting structures appear that have characteristics similar to the Jovian *S* bursts. In spite of noise, these structures seems to be quasi periodic with the Alfvén wave period (arrows).

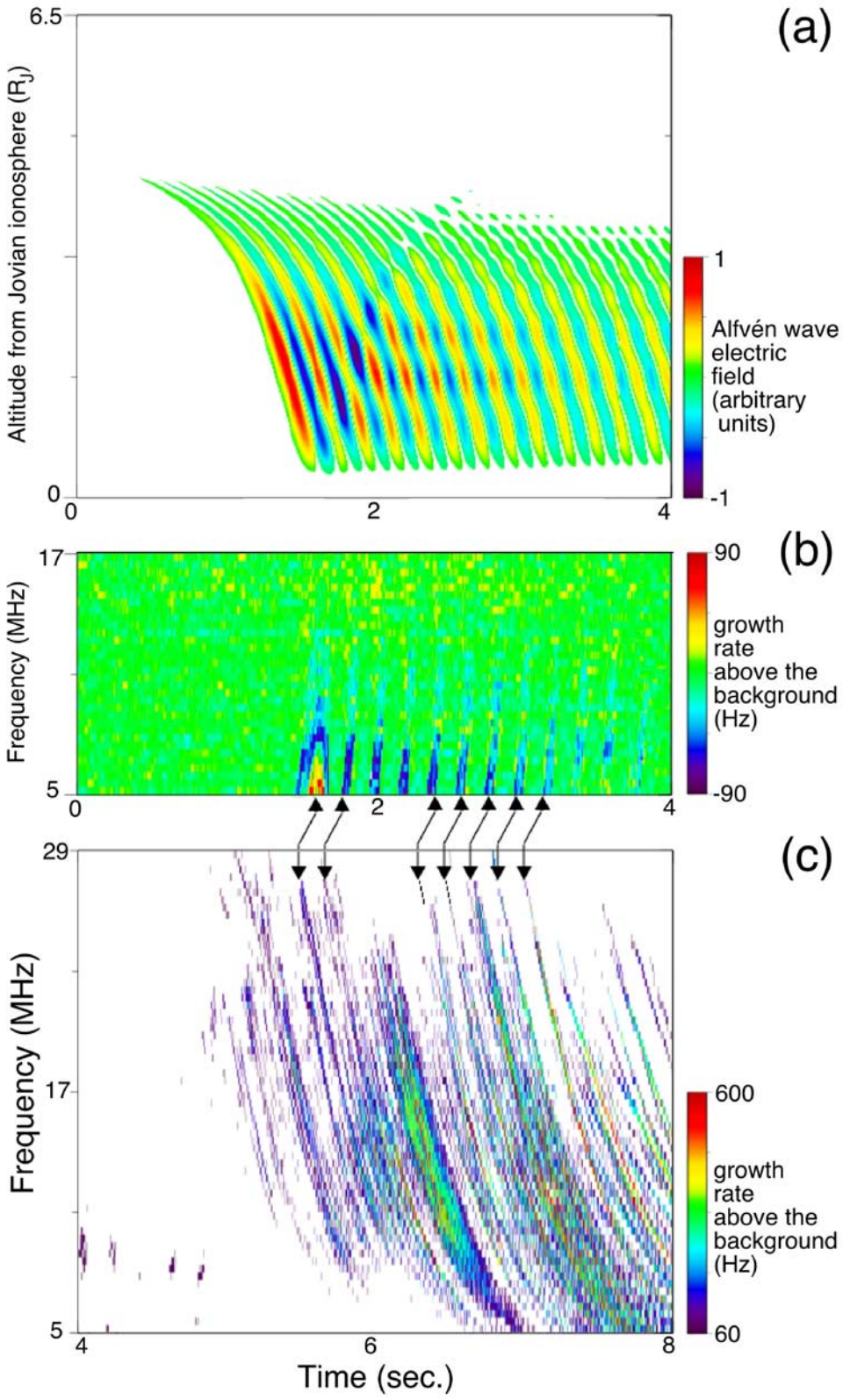

Figure 2

of the region producing the downgoing beam is therefore $\delta L \sim v\delta t \sim 3000$ km $\sim 0.04\ R_J$. We can conclude that the source of these downward electron beams, when compared to the Io-Jupiter flux tube length, is quite localized.

[23] This downward beam is at the origin of the shell-like distribution seen in Figures 3b and 3c. The upward beam seen in Figures 3b and 3c is the reflected part of the downward accelerated beam (the downward accelerated

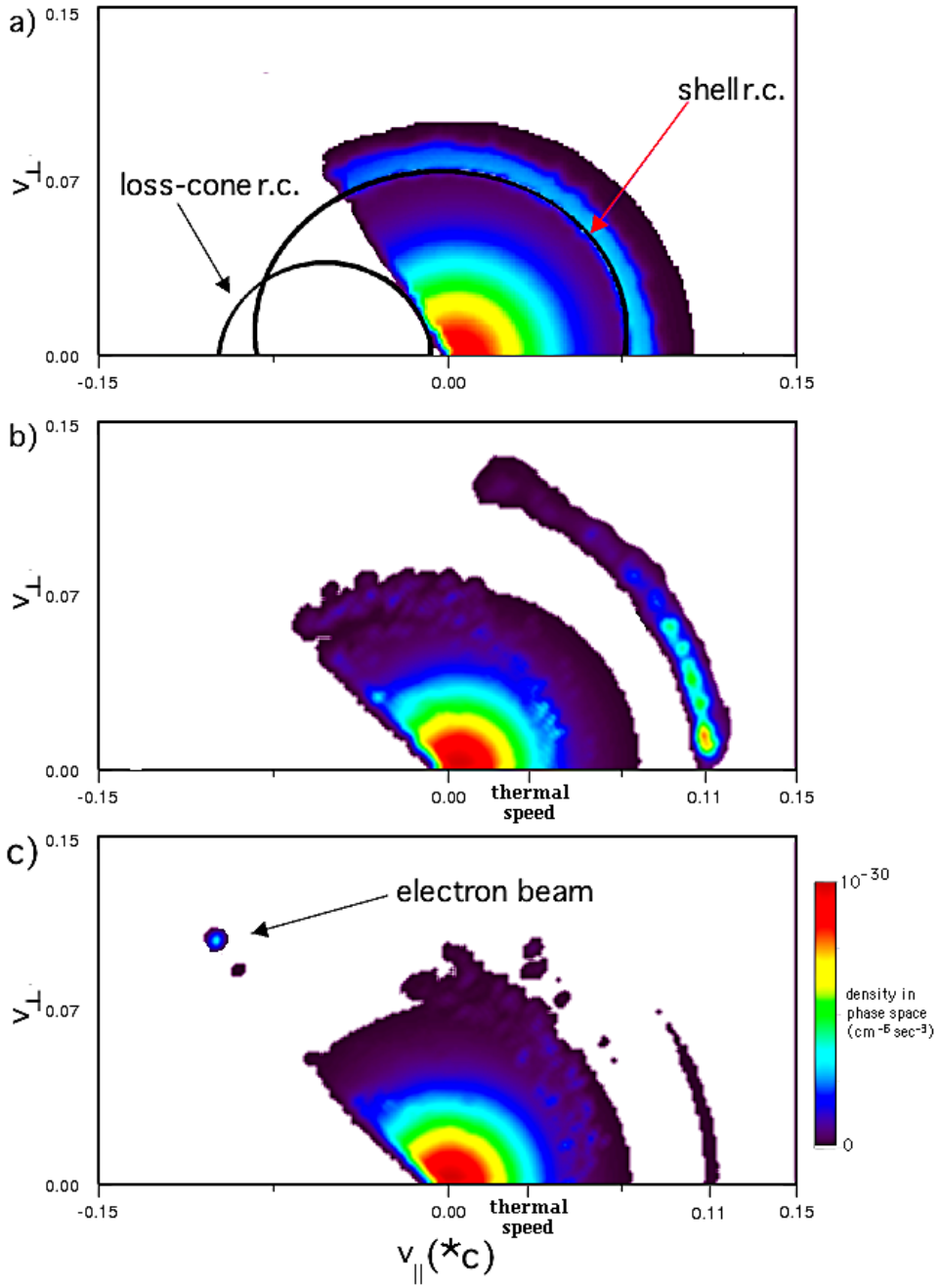

Figure 3. (a) Example of an unstable electron distribution relatively to the cyclotron-maser instability. The "loss cone" is due to magnetic mirror effect and loss by collisions in the ionosphere. The perpendicular gradient is positive along the loss cone border, and the resonance circle (r.c.) is tangent to it. A "shell" distribution is a ring of particles in the phase space. The resonance circle is tangent to its inner edge. (b and c) Distributions of the particles at different time of the simulation at an altitude of 0.1 R_J. Planetward accelerated electrons form an arc in the ($v_\parallel$, $v_\perp$) plane because of adiabatic motion and magnetic mirroring (Figure 3b). This arc is cut by the loss cone, generating antiplanetward electron beams moving adiabatically. These beams are nearly aligned with the loss cone border (Figure 3c). The time between Figures 3b and 3c exceeds the time particles need to travel to the planet and back, so the particles in the beams of the two figures are not the same. It explains why the beams do not reflect one another.

particles do not all have a null pitch angle and some of them,not trapped in Jupiter's ionosphere, bounce back, away from Jupiter.) This interpretation of our simulation is consistent with the modulation of the shell and near-loss cone beam at the AW frequency.

4. Cyclotron-Maser Growth Rate

[24] A complete description of the linear Cyclotron Maser Instability (CMI) theory is presented in the work of *Wu and Lee* [1979], *Wu* [1985], and *Galopeau et al.* [2004]. The latter authors deduce the Io "active" longitudes from CMI theory and magnetic field geometry. CMI occurs for electrons which fulfill the wave-particle resonance condition:

$$\omega = \omega_c/\Gamma - k_{\|} v_{\|} \tag{14}$$

where ω is the wave frequency, ω_c the electron cyclotron frequency and Γ the relativistic Lorentz factor. In the weakly relativistic approximation the wave-particle resonance condition is represented by a circle in the ($v_{\|}$, $v_{\perp}$) plane of center v_0 and radius R given by

$$\mathbf{v}_0 = c\frac{\mathbf{k}.\mathbf{b}}{k} \simeq \frac{k_{\|}c^2}{\omega_c}\mathbf{u}_{\|} \tag{15}$$

$$R = \sqrt{v_0^2 - 2\left(\frac{\omega}{\omega_c} - 1\right)}, \tag{16}$$

where $\mathbf{b}$ and $\mathbf{u}_{\|}$ are the unit vectors of the magnetic field and of the parallel velocity. The maser cyclotron growth rate γ is obtained by integration over the resonance circle of the particle distribution $f(\mathbf{v}_0, \mathbf{R}(\theta))$ gradient relative to the perpendicular velocity. $\mathbf{R}(\theta)$ is the vector radius of the resonance circle where θ is related to the parallel velocity axis. The solution of the equation of dispersion for nonrelativistic particles and for $|\omega| > |\gamma|$ is:

$$\gamma = \frac{\omega_p^2 c^2}{8\omega_c}\int_0^{2\pi} v_{\perp}^2(\theta)\nabla_{v_{\perp}} f(\mathbf{v}_0, \mathbf{R}(\theta))d\theta \text{ with } \omega > \omega_c \tag{17}$$

where ω_p is the electron plasma frequency.

[25] Positive growth rates require the gradient $\nabla_{v\perp} f(\mathbf{v}_0, \mathbf{R}(\theta))$ to reach positive values along a section of the resonance circle with a dominant contribution to the integral in equation (17). This is the case for "loss cone" and "shell" distributions (Figure 3a). In our simulation we compute the growth rates from the particle distributions along the field line for several resonance circle centers v_0 and radii R (which correspond to several frequencies ω and parallel wave vectors $k_{\|}$). Each of these circles corresponds to an extraordinary mode. Many of these modes are amplified. The mode that dominates the instability (in the linear approximation) is the most amplified. Therefore we retain the mode with the largest growth rate. The observed mode is the mode whose growth rate is the largest (mode which is the most amplified).

[26] Loss cone and shell instabilities growth rates are computed separately since their emission characteristics are quite different (beaming angle, wave velocity, etc.). Moreover the shell instability has a solution to the resonance condition (equation (14)) for $v_{\|} = 0$, implying $\omega < \omega_c$. Thus equation (17) is not accurate. An accurate computation of the shell instability growth rate involves a relativistic dispersion relation which is not taken into account here since there is no general solution for it [*Pritchett*, 1984]. Nevertheless we estimate the shell instability growth rates using equation (17). The exact shell instability growth rate should be lower than those computed with equation (17) since it depends strongly on the density ratio of the hot electron versus cold populations [*Pritchett*, 1984].

5. Results

5.1. Loss Cone Instability

[27] Figures 2b and 2c show the dynamic spectrum of the loss cone instability maximum growth rate. Figure 2b shows the first 4 s, during which no structure appears above 17 MHz, so we show only the results between 5 MHz and the latter frequency. Figure 2c shows the dynamic spectrum from 4 to 8 s. In both pictures the background (not zero but ~180 Hz because of the presence of the permanent loss cone) was subtracted. The negative value stands for growth rate lower than the background. In order to show clearly the radio structures, only growth rates above the background are shown after 4 s (in Figure 2c).

[28] We observe two kinds of structures. When Alfvén waves reach the emission region (between the second and the fifth seconds) low-frequency structures are generated by the waves propagation, and they appear mainly in absorption (the loss cone growth rate becomes lower than the background). The parallel electric field associated with the waves locally accelerate and decelerate the electrons (bulk acceleration), thus the structures appearing on the dynamic spectra are due to local perturbations of the whole electron distribution and not the electron beams. Since the parallel electric field amplitude decreases strongly toward the Jovian ionosphere, these structures appear only at low frequencies.

[29] The second kind of structures appears after 5 s. These are discrete, intense radio bursts that drift toward lower frequencies. Their drift rate averaged on the whole frequency range is ~17 MHz/s and decreases at low frequency, which is consistent with the observed *S* bursts drift rates [*Zarka et al.*, 1996; *Hess et al.*, 2007]. The study of the particle distributions (Figures 3b and 3c) in the emission region shows that these structures are generated by antiplanetward electron beams in adiabatic motion along the IFT.

[30] Interaction of particles with Aflvèn waves accelerate electrons in the parallel direction above Jovian ionosphere. Planetward accelerated electrons form an arc in the velocities plane, because of magnetic mirroring (Figure 3b). This arc is cut by the loss cone, generating antiplanetward electron beams with low spread of energy and pitch angle. These beams are nearly aligned with the loss cone border (Figure 3c) at every altitude, thus the electrons of the beams move adiabatically in the emission region (where the electric field is negligible). The beam velocity is about 0.11 c; that is, about 3 keV. It is consistent with the *S* bursts source motion inferred from observations in the above articles. Moreover it explains that the pitch angles of emitting

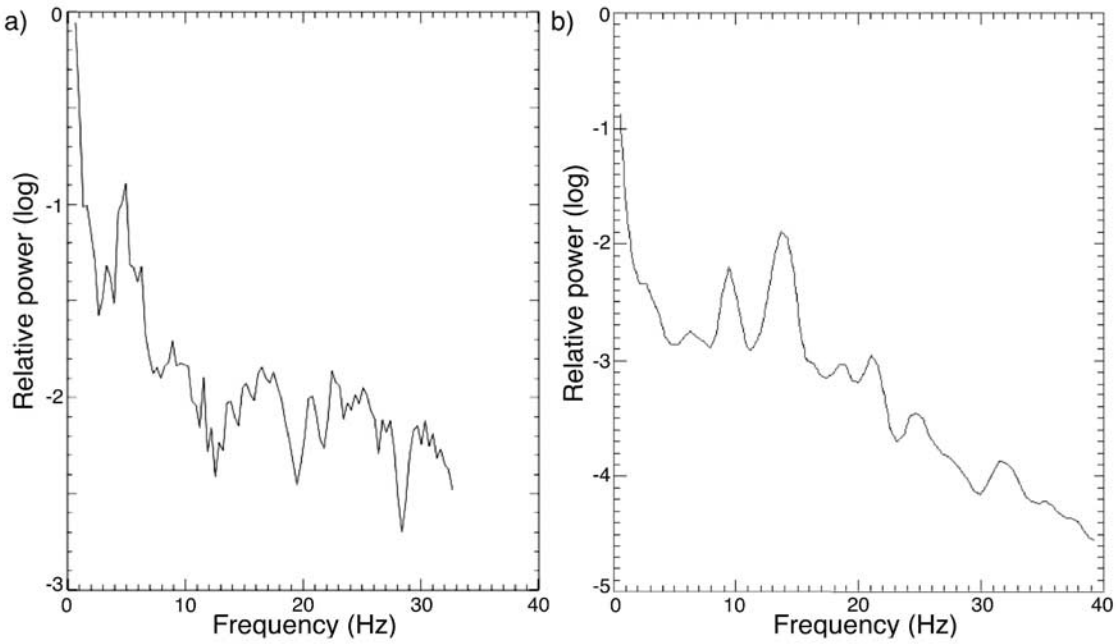

Figure 4. (a) Fourier transform over time of the dynamic spectrum of loss cone instability growth rates (from 5 to 8 s). It shows a maximum at a frequency of 5 Hz, which is consistent with the Alfvén waves frequency. The high amplitude of the lowest frequency is due to background value and to numerical noise. (b) Fourier transform over time of the dynamic spectrum is shown in Figure 1. Even if the bursts do not appear to be periodic on the dynamic spectrum, the Fourier transform shows a bump around 15 Hz; it corresponds to a mean time between each bursts of about 67 ms.

electrons found in the work of *Hess et al.* [2007] are nearly equal to the loss cone angle.

[31] The observation of the structure at the highest frequencies seems to show some quasi periodicity of the bursts, at the Alfvén wave frequency. Figure 4a shows a Fourier transform over time (and averaged over frequencies) of the dynamic spectrum of the loss cone instability (Figure 2c; from 5 to 8 s) in order to observe some quasi-periodicity of the radio bursts. It shows a maximum at 5 Hz, reminiscent of the Alfvén waves periodicity. Therefore the observed discrete structure is not the mere consequence of numerically induced noise, but it is related to the generation process that finds its origin in the propagation of kinetic Alfvén waves. Figure 4b shows the Fourier transform over time (and also averaged over frequencies) of the dynamic spectrum shown on Figure 1. The mean time between each bursts remains about 70 ms on the whole dynamic spectrum. The Fourier transform shows a bump around 15 Hz.

5.2. Shell Instability

[32] The shell instability dynamic spectrum (Figure 5) is noisy, since the number of particles seems to be too low to describe the distribution of the accelerated electron beams. Moreover, since the electron beams are generated above the emission region they have to reach the Jovian ionosphere before being reflected by magnetic mirror (Figure 3b). These downward beams do not generate radio waves by loss cone instability but they do by shell instability. Thus shell instability generates many drifting structures with both positive and negative slopes at the same time and frequency and the dynamic spectrum of the shell instability growth rate does not permit to identify structures as easily as for loss cone driven instability.

6. Discussion

[33] Our simulations show that electron acceleration by Alfvén waves can generate electron beams which can emit radio waves owing to cyclotron-maser instability. Magnetically mirrored (antiplanetward) beams, whose distribution is cut by the loss cone, emit radio bursts triggered by the loss cone instability. The characteristics of these radio bursts are consistent with those of the observed Jovian *S* bursts.

[34] 1. Discrete. The acceleration region is not located near the Io torus, as assumed by the Ellis model [*Ellis*, 1965], but in a region located just above the emission region (i.e., above 1 Jovian radius). It allows for short-lived electron beams, because they are close to the injection region, and thus discrete radio bursts. Radio bursts caused by electrons accelerated near the torus would be much more long-lived owing to the spread in the velocity of the electron beam from the near-Io acceleration region to the near-Jupiter emission region. Can we estimate the distance between the AW region that has a signature in the emission spectrum and the *S* bursts emission region? Looking at Figure 5, we can see that the time lag between the Alfvén waves injection emissions (at $t \sim 2$ s) and the first *S* burst is 3 s. The radio emission starts at $f = 32$ MHz, that corresponds to the cyclotron frequency just above the Jovian ionosphere (bottom of our simulation grid). Considering that the electron beam propagates at $v \sim 0.1$ c, the distance between the two regions is of the order of 1.25 R_J.

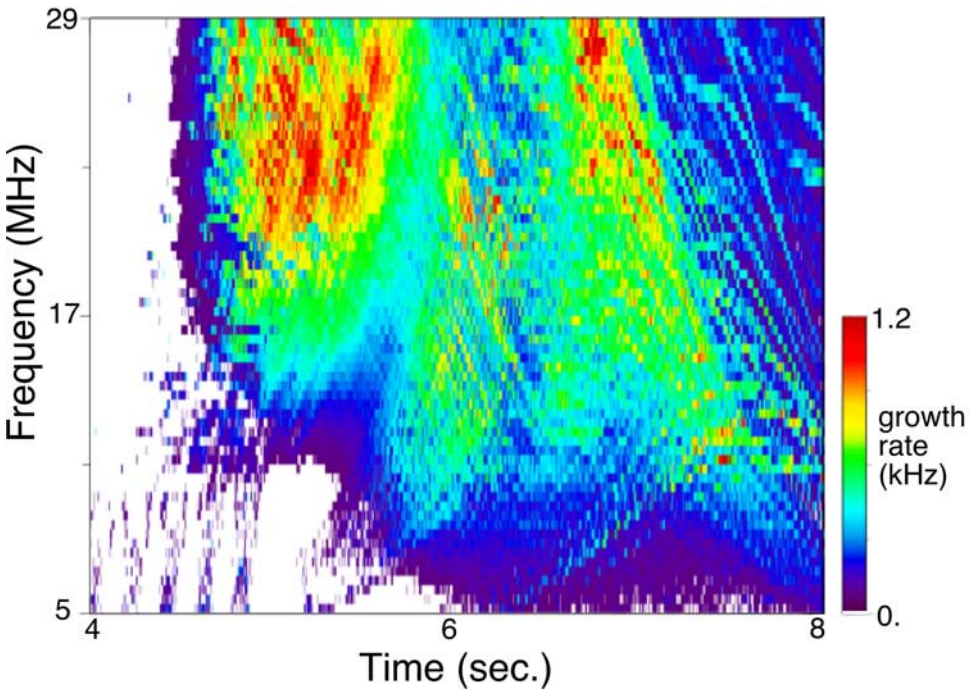

Figure 5. Dynamic spectrum of the shell instability growth rate from 4 to 8 s. Structures related to Alfvén wave propagation are visible at low frequency from 4 to 5 s. The shell instability is sensitive to both planetward and antiplanetward electron beams at the same time. Its dynamic spectrum shows a superposition of drifting structures with both positive and negative drift rates. No particular structures dominate on this figure. Although the growth rates seem to be slightly higher than the loss cone instability ones, they are overestimated since the relativistic corrections are not taken into account.

If the electron beam slow down by mirror effect is taken into account (estimated numerically), the distance becomes 0.9 R_J. We can see on Figure 2a that an altitude of 0.9 R_J corresponds to the region where the AW electric field begins to decrease.

[35] 2. Drifting in the time-frequency plane with a drift consistent with an adiabatic motion of the source. In the emission region, at least above 10 MHz (which is the lowest frequency well observed from the ground), the electric field due to Alfvén wave is negligible, then the electrons of the beam move adiabatically. This is consistent with *Zarka et al.* [1996]; *Hess et al.* [2007] who concluded to an adiabatic motion of the source from drift rate measurements. Moreover the electron energy of 3 keV in our simulation is consistent with the few keV found in the latter articles.

[36] 3. Quasi-periodic. The velocity of the Alfvén waves, at least in the acceleration region is far larger than the electron velocity, then the acceleration does not involve resonance between the particles and the Alfvén wave. The electron beam direction depends on the phase of the wave (positive or negative value of the electric field) and not on the direction of propagation of the wave. An Alfvén wave resonance near the Jovian ionosphere, presumed by *Su et al.* [2006]; *Ergun et al.* [2006], which generate antiplanetward waves could generate planetward electron beams as those generated in our simulation. The time and space resolutions in our simulation do not allow us to check this assumption up to now.

[37] In our simulation the *S* burst-like structures seem to be due to the loss cone instability, whereas shell instability leads to much more complex structures. As said in the previous sections this is due for a part to numerical noise, but it is mainly due to the fact that the shell instability is sensitive to both planetward and antiplanetward free energy sources. Some structures with a drift consistent with planetward sources are seen in the *S* burst observations but they represent only 1.5% of the observed bursts [*Zarka et al.*, 1996]. However, in our simulation, shell growth rates are over estimated and should be much lower than the loss cone driven instability. Further study and comparison to observations is required.

[38] *Hess et al.* [2007] have shown from experimental data that there often exists a potential drop of about 0.9 keV, located at altitudes around 0.1 R_J. These potential drops where not interpreted as the primary source of electron acceleration (as an energy of a few keV is needed). This potential drop cannot appear in our simulation, as it is a quasi static structure that do not depend on the AW propagation. However, we can notice that such potential drops (0.1 R_J) are situated bellow the AW electron acceleration region (0.9 R_J), and would impede a supplementary downward beam acceleration.

[39] **Acknowledgments.** We thank the referees for their helpful comments. The simulations were performed on the MPOPM computer of the IT service of the Paris observatory.

[40] Wolfgang Baumjohann thanks Yi-Jiun Su and Charles Higgins for their assistance in evaluating this paper.

References

Bagenal, F. (1994), Empirical model of the Io plasma torus: Voyager measurements, *J. Geophys. Res.*, *99*, 11,043–11,062.

Calvert, W., Y. Leblanc, and G. R. A. Ellis (1988), Natural radio lasing at Jupiter, *Astrophys. J.*, *335*, 976–985.

Carr, T. D., and F. Reyes (1999), Microstructure of Jovian decametric *S* bursts, *J. Geophys. Res.*, *104*, 25,127–25,142.

Carr, T. D., M. D. Desch, and J. K. Alexander (1983), Phenomenology of magnetospheric radio emissions, in *Physics of the Jovian Magnetosphere*, edited by A. J. Dessler, pp. 226–284, Cambridge Univ. Press, New York.

Connerney, J. E. P., M. H. Acuña, N. F. Ness, and T. Satoh (1998), New models of Jupiter's magnetic field constrained by the Io flux tube footprint, *J. Geophys. Res.*, *103*, 11,929–11,940.

Ellis, G. R. A. (1965), The decametric radio emission of Jupiter, *Radio Sci.*, *69D*, 1513–1530.

Ergun, R. E., Y.-J. Su, L. Andersson, F. Bagenal, P. A. Delemere, R. L. Lysak, and R. J. Strangeway (2006), *S* bursts and the Jupiter ionospheric Alfvén resonator, *J. Geophys. Res.*, *111*, A06212, doi:10.1029/2005JA011253.

Galopeau, P. H. M., M. Y. Boudjada, and H. O. Rucker (2004), Evidence of Jovian active longitude: 1. Efficiency of cyclotron maser instability, *J. Geophys. Res.*, *109*, A12217, doi:10.1029/2004JA010459.

Génot, V., P. Louarn, and F. Mottez (2000), Electron acceleration by Alfvén waves in density cavities, *J. Geophys. Res.*, *105*, 27,611–27,620.

Génot, V., P. Louarn, and F. Mottez (2004), Alfvén wave interaction with inhomogeneous plasmas: Acceleration and energy cascade towards small-scales, *Ann. Geophys.*, *22*, 2081–2096.

Goldreich, P., and D. Lynden-Bell (1969), Io, a Jovian unipolar inductor, *Astrophys. J.*, *156*, 59–78.

Hess, S., P. Zarka, and F. Mottez (2007), Io-Jupiter interaction, millisecond bursts and field-aligned potentials, *Planet. Space Sci.*, *55*, 89–99, doi:10.1016/j.pss.2006.05.016.

Kletzing, C. A. (1994), Electron acceleration by kinetic Alfvén waves, *J. Geophys. Res.*, *99*, 11,095–11,104.

Louarn, P. (1992), Auroral planetary radio emissions—Theoretical aspects, *Adv. Space Res.*, *12*, 121–134.

Lysak, R. L., and Y. Song (2003), Kinetic theory of the Alfvén wave acceleration of auroral electrons, *J. Geophys. Res.*, *108*(A4), 8005, doi:10.1029/2002JA009406.

Moncuquet, M., F. Bagenal, and N. Meyer-Vernet (2002), Latitudinal structure of outer Io plasma torus, *J. Geophys. Res.*, *107*(A9), 1260, doi:10.1029/2001JA900124.

Neubauer, F. M. (1980), Nonlinear standing Alfven wave current system at Io: Theory, *J. Geophys. Res.*, *85*, 1171–1178.

Prangé, R., D. Rego, D. Southwood, P. Zarka, S. Miller, and W. Ip (1996), Rapid energy dissipation and variability of the Io-Jupiter electrodynamic circuit, *Nature*, *379*, 323–325.

Pritchett, P. L. (1984), Relativistic dispersion, the cyclotron maser instability, and auroral kilometric radiation, *J. Geophys. Res.*, *89*, 8957–8970.

Queinnec, J., and P. Zarka (1998), Io-controlled decameter arcs and Io-Jupiter interaction, *J. Geophys. Res.*, *103*, 26,649–26,666.

Ryabov, B. P. (1994), Jovian *S* emission: Model of radiation source, *J. Geophys. Res.*, *99*, 8441–8449.

Saur, J. (2004), A model of Io's local electric field for a combined Alfvénic and unipolar inductor far-field coupling, *J. Geophys. Res.*, *109*, A01210, doi:10.1029/2002JA009354.

Su, Y., R. E. Ergun, F. Bagenal, and P. A. Delamere (2003), Io-related Jovian auroral arcs: Modeling parallel electric fields, *J. Geophys. Res.*, *108*(A2), 1094, doi:10.1029/2002JA009247.

Su, Y.-J., S. T. Jones, R. E. Ergun, and S. E. Parker (2004), Modeling of field-aligned electron bursts by dispersive Alfvén waves in the dayside auroral region, *J. Geophys. Res.*, *109*, A11201, doi:10.1029/2003JA010344.

Su, Y.-J., S. T. Jones, R. E. Ergun, F. Bagenal, S. E. Parker, P. A. Delamere, and R. L. Lysak (2006), Io-Jupiter interaction: Alfvén wave propagation and ionospheric Alfvén resonator, *J. Geophys. Res.*, *111*, A06211, doi:10.1029/2005JA011252.

Willes, A. J. (2002), Jovian *S* burst drift rates and *S* burst/*L* burst interactions in a phase-bunching model, *J. Geophys. Res.*, *107*(A5), 1061, doi:10.1029/2001JA000282.

Wong, H. K., and M. L. Goldstein (1990), A mechanism for bursty radio emission in planetary magnetospheres, *Geophys. Res. Lett.*, *17*, 2229–2232.

Wu, C. S. (1985), Kinetic cyclotron and synchrotron maser instabilities—Radio emission processes by direct amplification of radiation, *Space Sci. Rev.*, *41*, 215–298.

Wu, C. S., and L. C. Lee (1979), A theory of the terrestrial kilometric radiation, *Astrophys. J.*, *230*, 621–626.

Zaitsev, V. V., E. Y. Zlotnik, and V. E. Shaposhnikov (1985), Generation of the Jovian decameter *S* bursts, *Sov. Astron., Engl. Transl.*, *11*, 85–88.

Zarka, P. (1998), Auroral radio emissions at the outer planets: Observations and theories, *J. Geophys. Res.*, *103*, 20,159–20,194.

Zarka, P., T. Farges, B. P. Ryabov, M. Abada-Simon, and L. Denis (1996), A scenario for Jovian *S* bursts, *Geophys. Res. Lett.*, *23*, 125–128.

S. Hess and F. Mottez, Laboratoire de l'Univers et de ses Théories, Observatoire de Paris, Centre Nationale de Recherche Scientifique, 5 Place Jules Janssen, Meudon F-92125, France. (sebastien.hess@obspm.fr)

P. Zarka, Laboratoire d'Etudes Spatiales d'Instrumentation en Aerophysique, Observatoire de Paris, Centre Nationale de Recherche Scientifique, 5 Place Jules Janssen, Meudon F-92125, France.